JOURNAL OF MATERIALS SCIENCE 27 (1992) 3706–3718

Effect of sintering additives on the behaviour of SiC whisker-reinforced Si_3N_4 composites

W. KAI, J.-M. YANG, C. J. SHIH
Department of Materials Science and Engineering, University of California, Los Angeles, CA 90024, USA

A. EZIS
Cercom Inc., Vista, CA 92083, USA

The effects of sintering additives on the microstructural development, whisker stability, oxidation resistance and room-temperature mechanical properties of the SiC whisker-reinforced Si_3N_4 matrix composites were investigated. Seven different combinations of Y_2O_3 and Al_2O_3 were used as sintering additives. The composites containing 20 vol % SiC whiskers were densified by hot pressing. The microstructure of the resulting composites was characterized using X-ray diffraction, scanning and transmission electron microscopy. Oxidation testing of the composite at 1400 °C was conducted to investigate the relationship between matrix compositions and oxidation resistance. The flexural strength, fracture toughness and crack propagation patterns were also characterized and correlated with the microstructural features.

1. Introduction

Silicon nitride is one of the leading engineering ceramics for high-temperature structural applications due to its high strength at elevated temperatures, excellent oxidation resistance, low thermal expansion coefficient, good wear resistance, and light weight. However, its brittleness and high sensitivity to flaws remain the main hindrances to its wider applications [1–3]. The current direction toward developing these materials is to improve both reliability and properties through a composite approach. SiC whiskers have been added into an Si_3N_4 matrix as a reinforcing phase to improve its toughness and strength. Typical processing techniques, such as hot-pressing (HP), hot isostatic pressing (HIP), pressureless sintering, and reaction bonding are used to densify the composites [4–7]. However, due to strong covalent bonds and low self-diffusivity of Si_3N_4, the classical solid-state sintering techniques are unable to densify the Si_3N_4. In order to densify the Si_3N_4, appropriate sintering aids must be used to promote liquid-phase sintering via solution–precipitation processes [8]. Most metal oxides, such as MgO, La_2O_3, Ce_2O_3, Y_2O_3, and Al_2O_3 are common sintering aids. However, the amount and type of sintering additives affect the amount and viscosity of the liquid, which will, in turn, affect densification as well as grain coarsening and mechanical properties of the resulting Si_3N_4. A previous study also indicated that sintering additives affected the stability of SiC whiskers [9]. Therefore, to develop a strong and tough SiC whisker-reinforced Si_3N_4 composite, it is necessary to optimize the amounts and types of sintering additives.

The purpose of the present work was to study the effect of sintering additives on the behaviour of SiC whisker-reinforced Si_3N_4 composites. Y_2O_3 and Al_2O_3 were chosen as sintering additives. Y_2O_3 is a devitrification agent, stimulating the nucleation and growth of crystalline phases in the amorphous boundary. Al_2O_3 was used to reduce the softening temperatures of the residual amorphous phase. SiC whiskers, along with different amounts of sintering additives, are added to Si_3N_4 and densified using a hot-pressing technique. The influences of sintering additives on the microstructural development of the Si_3N_4 matrix and stability of SiC whiskers are studied.

2. Experimental procedure

2.1. Materials and processing

The Si_3N_4 powders with particle sizes ranging from 0.3–8 μm were used as the matrix materials in this study. The SiO_2 content of the Si_3N_4 powder surfaces was found to be around 2.99% by chemical solution method (25 mol % concentrated HF) at 70 °C. The SiC whiskers were used as reinforcement. High-purity Y_2O_3 and Al_2O_3 powders were used as sintering additives. The seven different matrix compositions examined in this study are listed in Table I. The procedures for fabricating the composites are outlined as follows. The Si_3N_4 powders with different amount of Y_2O_3 and Al_2O_3 powders were first wet milled. The SiC whiskers (20 vol %) were then introduced into the slurry, and dispersed through wet milling in isopropyl alcohol. The slurry was then dried, dry milled and cold

0022–2461

TABLE I Compositions of HP-SiC_w/Si_3N_4 composites[a]

Mixing powder grade	Si_3N_4 (wt %)	Y_2O_3 (wt %)	Al_2O_3 (wt %)
A	97.75	2.00	0.25
B	95.50	4.00	0.50
C	93.25	6.00	0.75
D	91.00	8.00	1.00
E	88.75	10.00	1.25
F	86.50	12.00	1.50
G	82.00	15.00	3.00

[a] Each composite contained 80 vol % mixing powders with 20 vol % SiC whiskers.

formed into 15 cm × 15 cm plates. The powder compacts were densified by controlling at 35 MPa pressure in a graphite die which was heated in a furnace at 1750 °C for 3 h in a reduced nitrogen atmosphere. All of the composites were densified under the same conditions.

2.2. Microstructural characterization

The densities of the composites were measured using a helium autopycnometer (Micromeritics Model 1320). Optical and electron microscopy were used to characterize the microstructure and morphology of the composite. In addition, the detailed microstructure of the SiC whiskers and composites were analysed by transmission electron microscopy (Joel 100 CX) with selected-area diffraction pattern (SAD). To prepare the TEM sample, the SiC whiskers were dispersed in acetone to form a liquid solution. A droplet of this solution was placed on the copper grid and dried on a hot plate at 100 °C. The grid was then coated with a thin layer of carbon before observation. For the composite specimens, conventional mechanical polishing was used, followed by ion milling with an argon dual-beam at 5.5 kV and 5 mA to perforation. A thin layer of carbon was also coated on the samples to eliminate surface charging before observation.

X-ray diffraction analysis (monochromatic CuK_α radiation) was used to study the phases present in the composites. In order to eliminate the preferred orientation, avoid the microabsorption effect, and precisely determine the quantitative contents of each phase, the composite specimens were ground to 325-mesh powders (about 70 μm). X-ray analysis was run at 35 kV with 0.02° angle increment per 2 s scanning time. The relative intensities of the first four strong peaks of different phases were used for the quantitative analysis. The procedures for the quantitative determination of the phase content can be found in [10].

The thermal expansion coefficient of the composite was measured by Orton Automatic Recording Dilatometer (Model 15BC-1) with Linseis Recorder (Model LY-18100). The dilatometer was heated to 300 °C at a rate of 1 °C min^{-1}, and followed by 3 °C min^{-1} to 1400 °C. After 1 h at 1400 °C, the dilatometer was cooled down to room temperature at 3 °C min^{-1}. The thermal expansion coefficients were calculated between 20 and 1000 °C and 20 and 1400 °C, respectively. After thermal expansion measurement, the oxide scales on the surface of each specimen were also examined using SEM and X-ray diffraction analysis.

2.3. Mechanical testing

The specimens for mechanical testing were prepared from each composite plate with the tensile surface perpendicular to the loading direction. Flexural strength was determined by three-point bending tests on 25 mm × 5 mm × 3 mm test specimens. Fracture toughness was also determined by three-point bending tests on 25 mm × 3 mm × 6 mm test specimens. The chevron notch was cut parallel to the hot-pressed direction using a low-speed diamond saw. The depth of notch was controlled to about 45%–55% of the specimen depth, which was recommended by the ASTM standard [11]. All the tests were conducted in an Instron machine with a crosshead speed of 0.5 mm min^{-1}. At least seven bars were tested to obtain the flexural strength and fracture toughness.

In order to study the crack propagation and fracture behaviour of ceramic composites, indentation tests were also conducted using a Vickers indentor. The loads used to generate the crack varied from 15–45 kg. A minimum of four indented points were made by each load and four different loadings were applied. The crack lengths and diagonal lengths were directly measured by optical microscopy using × 40 magnification. Fracture toughness was determined by the semi-crack model [12]

$$K_{IC} = 0.016(E/H)^{1/2}(P/C^{3/2}) \quad (1)$$

where C is the radius of crack length, H is the hardness value calculated from the diagonal length, P is the load, and E is the Young's modulus of the composites.

3. Results and discussion

3.1. Microstructural characterization

The X-ray diffraction analyses of the starting Si_3N_4 powder and SiC whiskers are shown in Fig. 1. The Si_3N_4 powder contained both α (90%) and β (10%) phases. The β-SiC whiskers had a straight, long rod-like shape and high aspect ratio (length to diameter) as shown in Fig. 2a. The typical node structure was clearly observed. The details of whisker morphology are given by bright- and dark-field transmission electron micrographs in Fig. 2b and c. The node structures were formed from stacking faults, which were typically perpendicular to the whisker long-axis.

The densities of the composites with different amounts of sintering additives measured using an autopycnometer are listed in Table II. All of the composites had densities higher than 3.1 g cm^{-3} indicating that the composites were densified using these sintering additives. The differences in density among these composites may be attributed to the presence of different oxynitride phases, which had different densities. The deep-etched micrographs of the composites are shown in Fig. 3. The whiskers (W) were easily distinguished from the elongated β-Si_3N_4 by means of

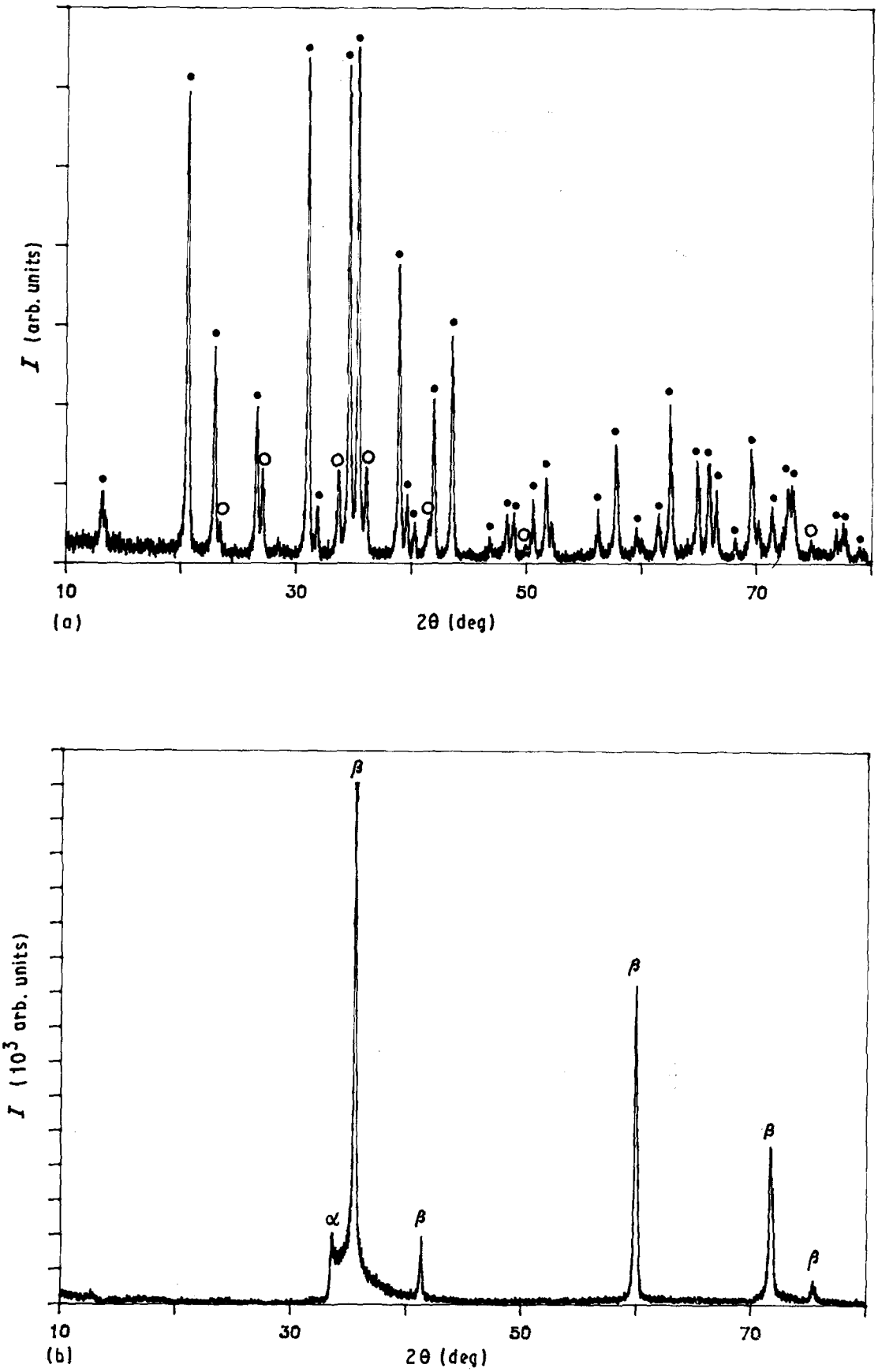

Figure 1 XRD analysis of starting materials: (a) Si_3N_4 powders (●) α-Si_3N_4, (○) β-Si_3N_4, (b) SiC whiskers.

their node structures. The grain size of the composites was found to be approximately 2–3 μm.

The phases present and relative amounts of the β-Si_3N_4, SiC and crystallized second phases in the as-processed composites analysed by X-ray diffraction are given in Table III. A typical X-ray diffraction pattern is shown in Fig. 4. The results indicate that the α-Si_3N_4 has completely converted to β-Si_3N_4 during hot-pressing. Three different crystallized second phases in the matrix were identified: Si_2N_2O (composition A, B), α-$Y_2Si_2O_7$ (composition B, C), and $Y_{10}Si_6O_{24}N_2$ (H phase, composition D–G). The mole

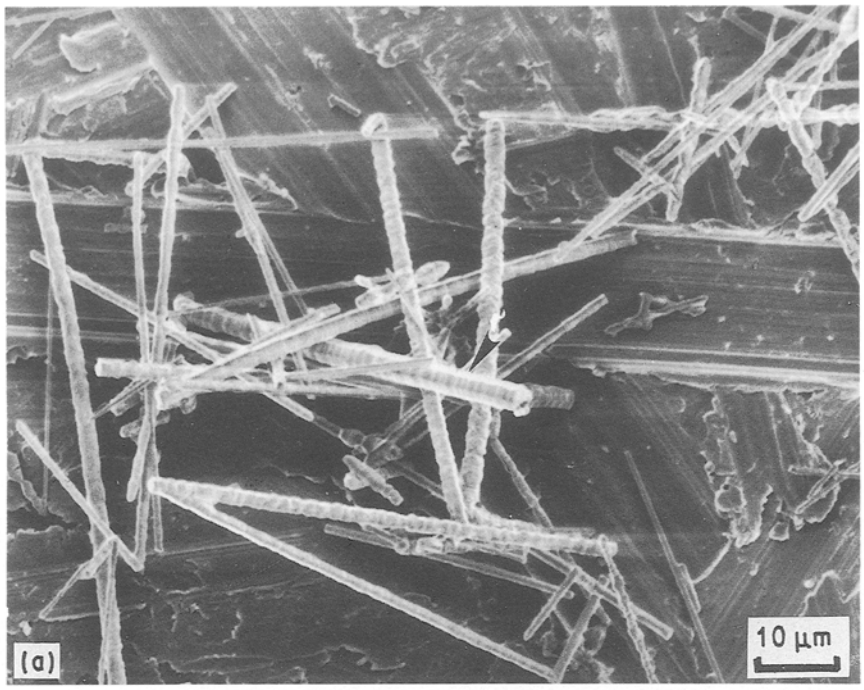

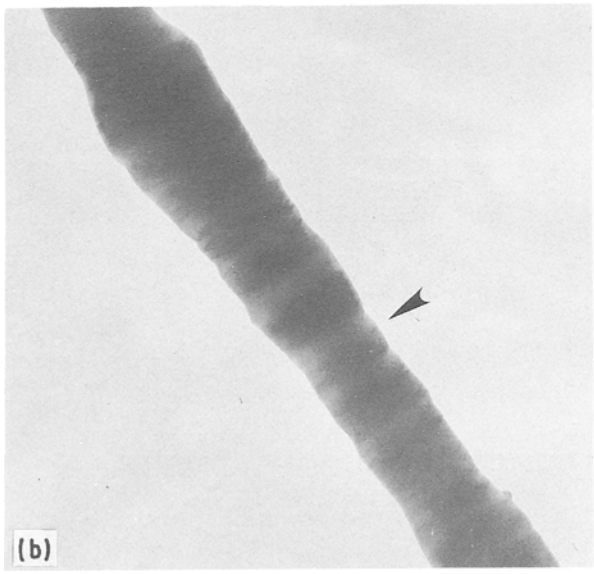

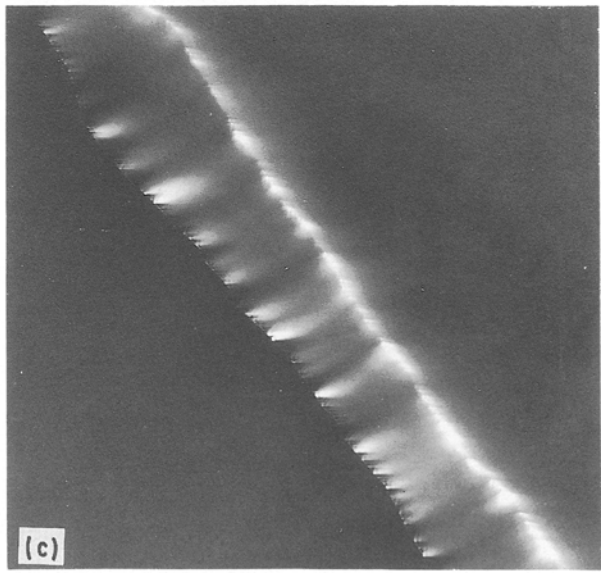

Figure 2 (a) The geometry and surface morphology of SiC whiskers. (b, c) Transmission electron micrographs showing stacking faults on the whiskers in bright and dark field × 26 000.

TABLE II Density data of HP-SiC_w/Si_3N_4 composites with different sintering additives

Composite grade	Density ($g\,cm^{-3}$)		Theoretical density (%)
	Measured[a]	Calculated[b]	
A	3.186	3.220	98.94
B	3.189	3.240	98.43
C	3.228	3.261	98.99
D	3.271	3.282	99.66
E	3.263	3.303	98.79
F	3.434	3.324	100
G	3.451	3.363	100

[a] All the measured data had the standard deviation less than 0.06% of the values.

[b] The calculated density was based on the density of the starting materials (listed in Table II).

fractions of yttria atoms in the composite before and after processing were calculated and are given in Table IV. The results showed that the number of yttrium atoms found in these crystallized phases is less than that in the starting powder. In addition, the aluminium-containing crystallized second phase was not detected by the X-ray diffraction. Therefore, some aluminium-containing and yttrium-containing amorphous grain-boundary phases are present in the composites which cannot be identified by X-ray diffraction [13].

It is obvious that different amounts of sintering additives result in different amounts and types of grain-boundary phases. The formation of different crystalline phases can be explained by examining the

Si_3N_4–Y_2O_3–SiO_2 phase diagram shown in Fig. 5 [14]. When the amount of sintering additives is low, the presence of a high amount of SiO_2 (~ 3 wt %) on the surface of the Si_3N_4 powder and a high free-oxygen content of the SiC whiskers (2.85 wt %) will keep the crystallized second phase in the SiO_2–Si_2N_2O–$Y_2Si_2O_7$ triangle-phase region. However, when the amount of sintering additives is increased, the amount of Si_3N_4 powder and SiO_2 on its surfaces would decrease. As a result, the second phases would shift from the Si_3N_4–$Y_2Si_2O_7$–SiO_2 compatibility triangle to the Si_3N_4–$Y_2Si_2O_7$–$Y_{10}Si_6O_{24}N_2$ compatibility triangle.

The amounts of SiC whisker retained in the composite obviously decreased after hot-pressing (as shown in Table III), indicating whisker degradation. A previous study indicated that the SiC whisker reacted with nitrogen and was converted to Si_3N_4 during hot isostatic pressing at high nitrogen pressures [15]. However, thermodynamic calculations indicate that the SiC whisker is stable under the current processing conditions. Furthermore, the results from Table III showed that the extent of whisker degradation varied with matrix composition. It appears that the sintering additives will affect the stability of the SiC whiskers. This may be associated with the presence of liquid oxynitride during hot pressing. Based upon the amount of Y_2O_3, Al_2O_3 and SiO_2 (from the Si_3N_4

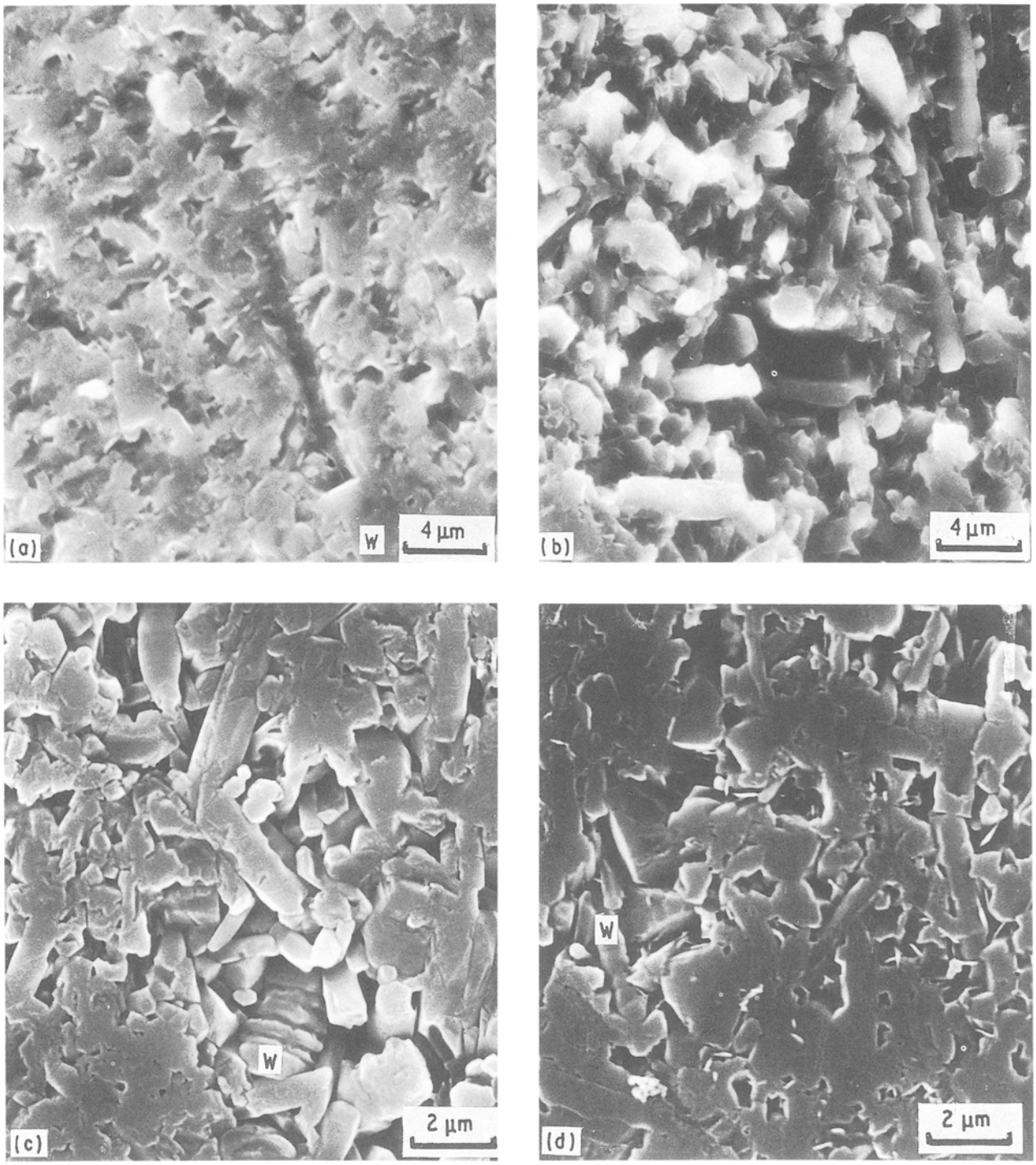

Figure 3 (a–g) Typical etching morphology of SiC_w/Si_3N_4 composites W, Whiskers in different composites A–G, respectively.

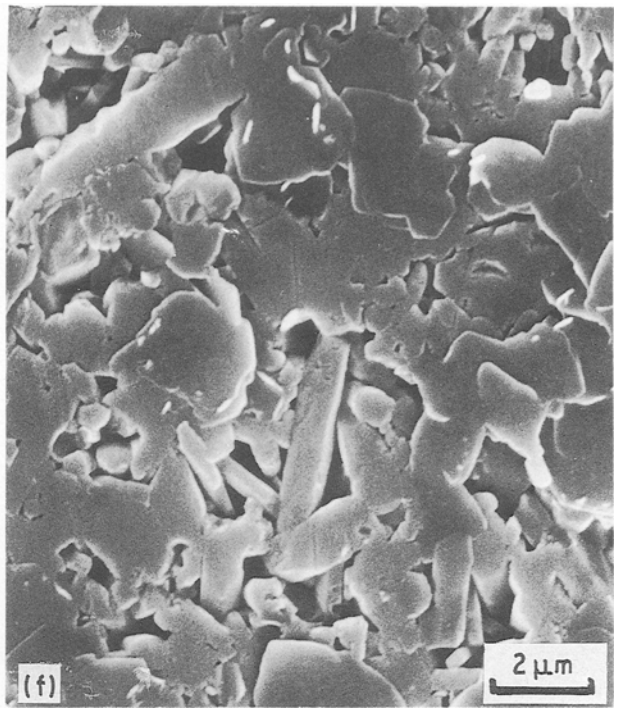

Figure 3 Continued.

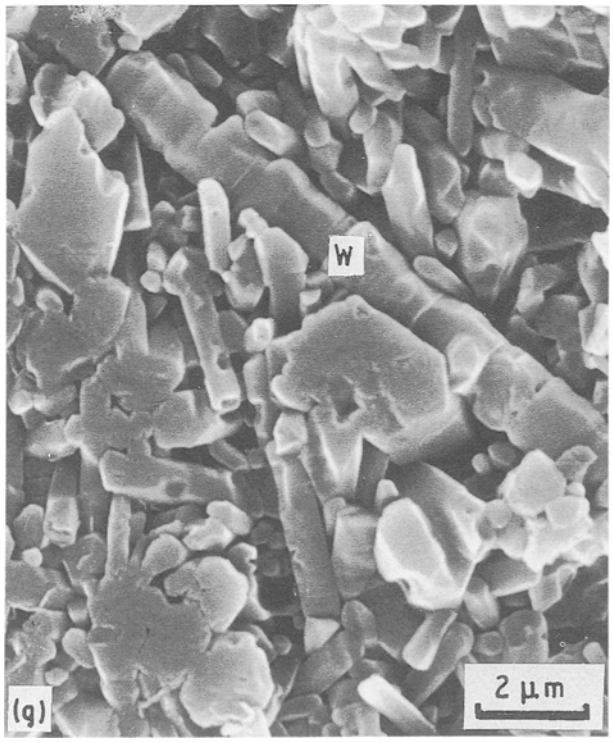

TABLE III X-ray diffraction and quantitative analysis of HP-SiC_w/Si_3N_4 composites[a]

Composite grade	Y_2O_3/Al_2O_3 ratio	Major phases (wt %)	Second crystallized phases[b] (wt %)
A	2/0.25	β-Si_3N_4 (79.59) β-SiC (12.95)	Si_2N_2O (7.46)
B	4/0.50	β-Si_3N_4 (78.80) β-SiC (10.36)	Si_2N_2O (6.57) α-$Y_2Si_2O_7$ (4.27)
C	6/0.75	β-Si_3N_4 (81.66) β-SiC (15.01)	α-$Y_2Si_2O_7$ (3.25)
D	8/1.00	β-Si_3N_4 (82.21) β-SiC (16.13)	$Y_{10}Si_6O_{24}N_2$ (1.66)
E	10/1.25	β-Si_3N_4 (76.41) β-SiC (13.58)	$Y_{10}Si_6O_{24}N_2$ (4.62) α-$Y_2Si_2O_7$ (5.39)
F	12/1.50	β-Si_3N_4 (78.33) β-SiC (12.73)	$Y_{10}Si_6O_{24}N_2$ (8.94)
G	15/3.00	β-Si_3N_4 (77.26) β-SiC (11.65)	$Y_{10}Si_6O_{24}N_2$ (11.09)

[a] The molecular weight (M_W) of all the phases was listed as: Si_3N_4 140 g mol^{-1}, SiC 40.09 g mol^{-1}, Si_2N_2O 100.00 g mol^{-1}, $Y_2Si_2O_7$ 345.82 g mol^{-1}, $Y_{10}Si_6O_{24}N_2$ 1469.10 g mol^{-1}, Y_2O_3 225.82 g mol^{-1}, Al_2O_3 102.02 g mol^{-1}.

[b] The density of β-Si_3N_4, β-SiC, Y_2O_3, Al_2O_3, Si_2N_2O, α-$Y_2Si_2O_7$, and $Y_{10}Si_6O_{24}N_2$ was 3.192, 3.217, 5.03, 3.90, 2.84, 4.45, 4.69 (g cm^{-3}), respectively. These data were used to convert the volume fraction to weight fraction for each phase.

powder surface and SiC whiskers), the liquidus temperature of each composition can be calculated. The results are shown in the Y_2O_3–Al_2O_3–SiO_2 phase diagram (Fig. 6). It is clear that higher amounts of sintering additives will raise the liquidus temperature. This, in turn, will affect the viscosity of the liquid oxynitride and the α–β Si_3N_4 conversion from the liquid phase. These factors may ultimately influence the stability of SiC whiskers either through dissolution or solid–liquid reactions.

Typical transmission electron micrographs of the composites are shown in Figs 7 and 8. The β-Si_3N_4, SiC whisker, crystallized and amorphous grain-boundary phases were clearly identified. The SAD patterns of the β-Si_3N_4 and H phases are shown in Fig. 7b and c. Some matrix defects, such as twins (Fig. 8b) and dislocations (Fig. 8c) may also be observed, which have been reported previously [16]. In addition, a thin glassy layer (< 20 nm) was also observed near the whisker surface (Fig. 8d) and between the matrix and the dark glassy phase (Fig. 8e).

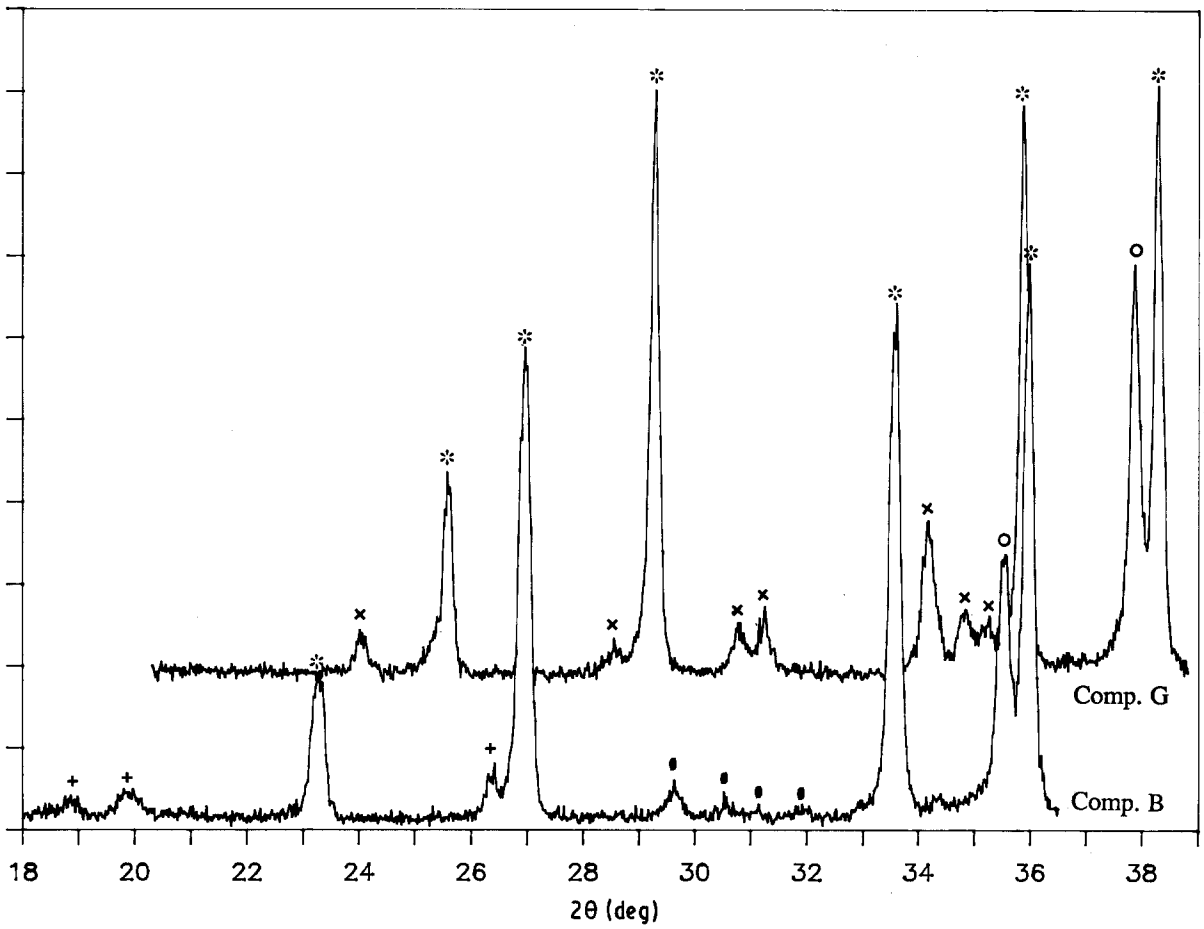

Figure 4 XRD analysis of SiC_w/Si_3N_4 composites. (*) β-Si_3N_4, (○) β-SiC, (+) Si_2N_2O, (⌀) α-$Y_2Si_2O_7$, (×) $Y_{10}Si_6O_{24}N_2$.

TABLE IV The mole fractions of yttrium atoms for both starting materials and as-processed composites[a]

Composite grade	Yttrium atoms on starting powders (mol %)	Second crystallized phases containing yttrium atoms (total mol %)
A	0.0137	none
B	0.0276	0.0275
C	0.0416	0.0194
D	0.0560	0.0114
E	0.0704	0.0694[b]
F	0.0852	0.0673
G	0.1074	0.0889

[a] All the mol % Y atoms were calculated from the XRD-quantitative results in Table III.
[b] The mol % Y atoms for both α-$Y_2Si_2O_7$ and $Y_{10}Si_6O_{24}N_2$ were counted.

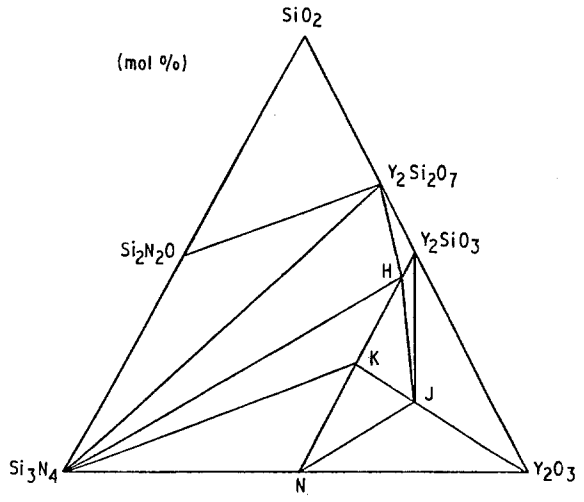

Figure 5 Phase diagram of Si_3N_4–Y_2O_3–SiO_2 [14]. H, $Y_{10}Si_6O_{24}N_2$; J, $Y_4Si_2O_7N_2$; K, $YSiO_2N$; N, $Y_2Si_3O_3O_4$.

3.2. Thermal expansion behaviour and oxidation resistance

The thermal expansion coefficients of the composites with different sintering additives were calculated from the slope of elongation versus temperature curves. The CTE data between 20–1000 °C and 20–1400 °C are tabulated in Table V. All the CTE values were between 3.3 and $4.7 \times 10^{-6}\,°C^{-1}$, which are the thermal expansion coefficients of Si_3N_4 and SiC, respectively. In addition, the CTE data of second phases for the Si_2N_2O, $Y_2Si_2O_7$, $Y_{10}Si_6O_{24}N_2$ were reported to be about 4.4, 8.0, $8.2 \times 10^{-6}\,°C^{-1}$, respectively [17–20]. It is clear that sintering additives affect the CTE of the resulting composites because of the formation of different second phases. The typical scanning electron micrographs of the surfaces of the composites after CTE measurement are given in Fig. 9a–c. A porous oxide layer was found on the surface on the composite as shown in Fig. 9a. The thickness of the porous oxide layer was found to be around 20 μm (Fig. 9b). The detailed morphology of the oxide scale on the oxidized surface is illustrated in Fig. 9c.

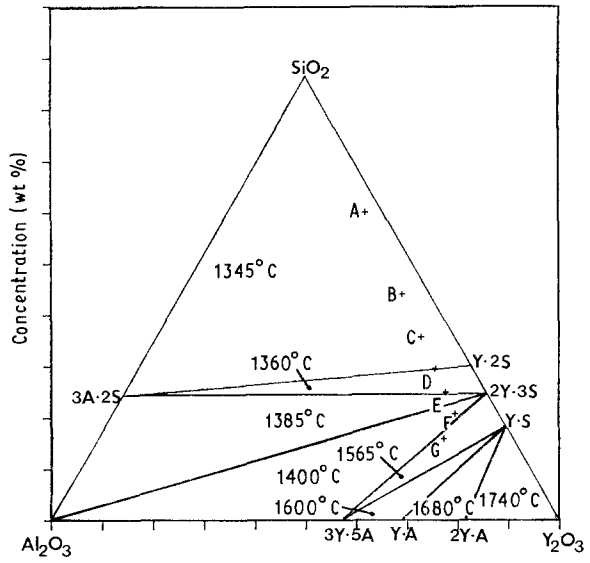

Figure 6 Phase relationships and liquidus temperature in the Y_2O_3–Al_2O_3–SiO_2 system for composites A–G.

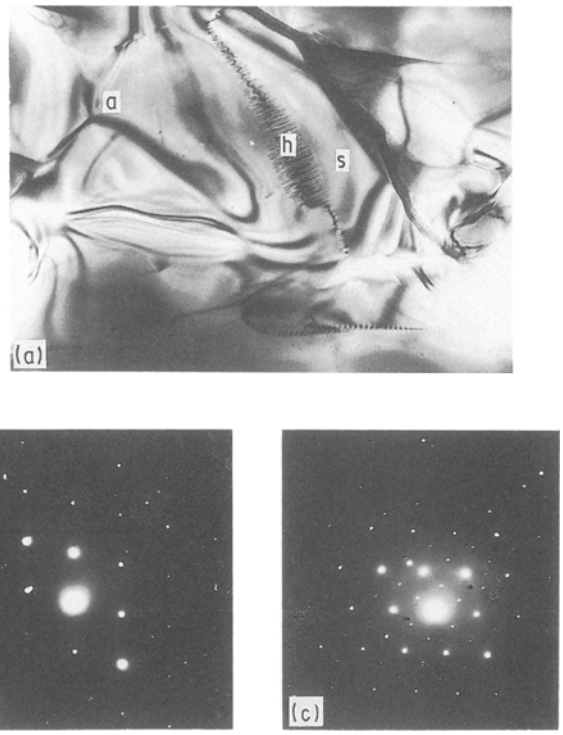

Figure 7 (a) Transmission electron micrographs of SiC_w/Si_3N_4 composites (composition D) × 33 000; a, amorphous phase; h, $Y_{10}Si_6O_{24}N_2$ (H) phase; s, Si_3N_4 matrix; (b) SAD pattern of Si_3N_4 matrix, $Z = [0\,1\,1\,1]$; (c) SAD pattern of H phase, $Z = [1\,2\,1\,3]$.

The crystal structure of the oxide scale on the surface of each specimen after thermal expansion testing was studied by X-ray diffraction (XRD). A typical X-ray diffraction pattern is shown in Fig. 10. The crystallized second phases in these composites were identified and are also listed in Table V. The Si_2N_2O phase was retained for all the composites at 1400 °C. The β-$Y_2Si_2O_7$, instead of α-$Y_2Si_2O_7$ phase was found in all of the composites. In addition, two different SiO_2 phases, cristobalite and coesite, were found on the surface of the specimens. However, the H-phase in composites with composition: E, F, and G was not detected. It appeared that H-phase was decomposed at 1400 °C in air. The XRD results for each composite at 0.1 mm below the surface after CTE test are also given in Table V. The crystallized second phases in these composites remained the same as those found in the as-processed state except in composite D. In composite D, the crystallized second phase was found to be β-$Y_2Si_2O_7$ instead of $Y_{10}Si_6O_{24}N_2$.

The formation of β-$Y_2Si_2O_7$ might be due to the phase transformation or chemical reactions. The phase transformation between α and β-$Y_2Si_2O_7$ was reported to occur around 1400 °C [20]. Therefore, it is

TABLE V The results of thermal expansion coefficients and second crystallized phases for both the surface and 0.1 mm below the surface of SiC_w/Si_3N_4 composites after CTE measurements

Composite grade	CTE data (10^{-6} °C^{-1})		Second crystallized phases[a] by XRD analysis	
	20–1000 °C	20–1400 °C	Surface	0.1 mm below the Surface
A	3.76	4.50	SNO, O_7, SO1, SO2 (tr.)[b]	SNO, SO1 (tr.), SO2 (tr.)
B	3.75	4.31	SNO, O_7, SO1, SO2 (tr.)	SNO, O_7 (tr.) SO1 (tr.), SO2 (tr.)
C	4.00	4.55	SNO, O_7, SO1, SO2	O_7 (tr.), SO1, SO2
D	4.01	4.61	O_7, SO1, SO2 (tr.)	O_7, SO1 (tr.), SO2 (tr.)
E	4.01	4.37	O_7, SO1	O_7, H (tr.)
F	4.02	4.72	O_7, SO1	O_7, H
G	3.90	4.45	O_7, SO1	H, one unknown peak

[a] SNO = Si_2N_2O, silicon oxynitride. O_7 = β-$Y_2Si_2O_7$, yttrium disilicate. SO1 = SiO_2, cristobalite (silica). SO2 = SiO_2, coesite (silica). H = $Y_{10}Si_6O_{24}N_2$, yttrium silicon oxynitride.
[b] tr. = trace amount in XRD results of that sample.

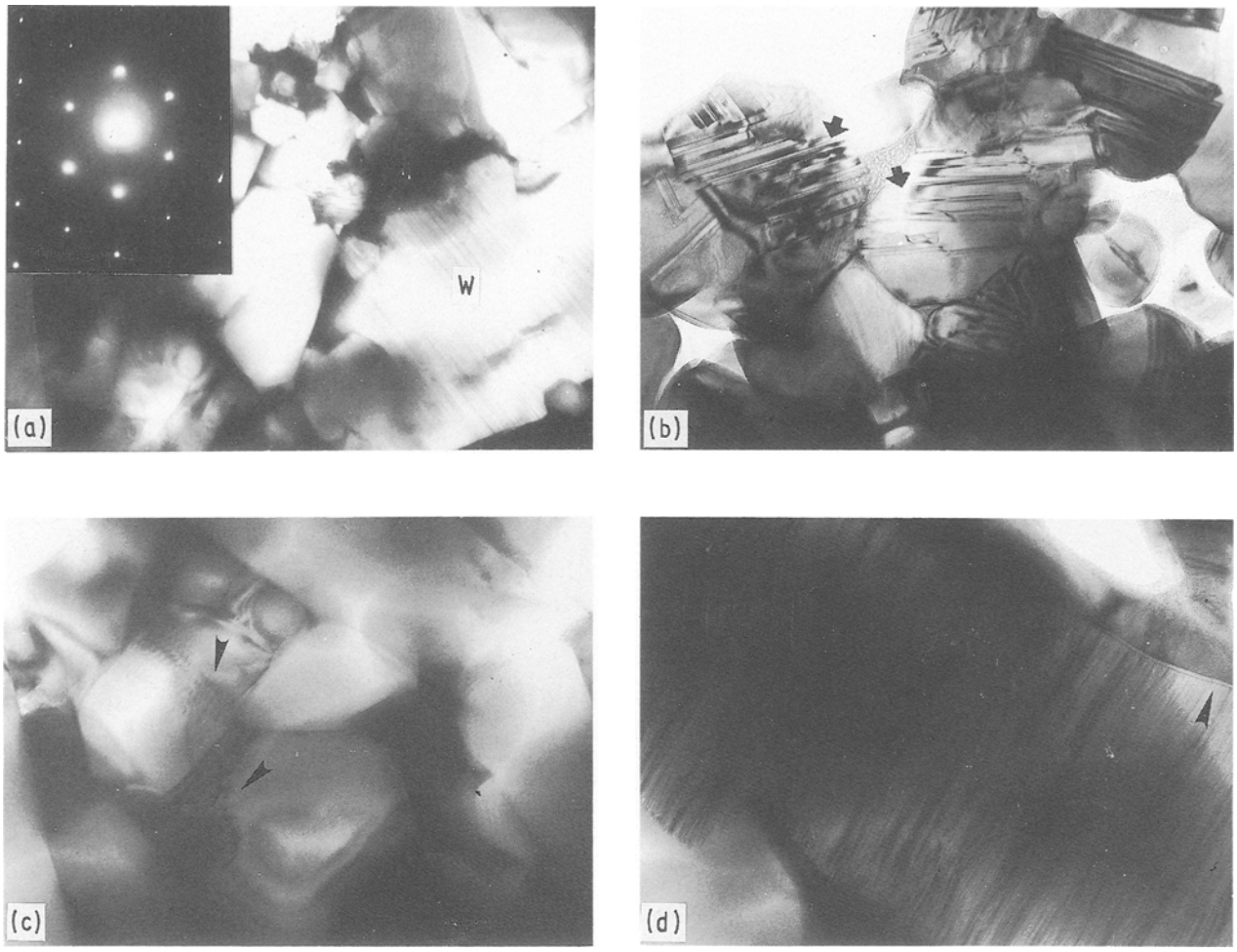

Figure 8 (a) Transmission electron micrographs of SiC whisker in SiC_w/Si_3N_4 composites in Si_3N_4 matrix, (d) a thin layer near the whisker surface, (e) a thin layer between the Si_3N_4 matrix and the glassy phase (G). (a) × 20 000, (b–d) × 66 000, (e) × 50 000.

expected that phase transformation will take place in the composites containing β-$Y_2Si_2O_7$ second phase (compositions A, B, C, E). In addition, in the composites containing $Y_{10}Si_6O_{24}N_2$ second phase (compositions D, E, F, G), β-$Y_2Si_2O_7$ may form through the following reaction

$$Y_{10}Si_6O_{24}N_2 + 4SiO_2 + 1.5O_2 \rightarrow 5Y_2Si_2O_7 + N_2 \quad (1)$$

However, the $Y_{10}Si_6O_{24}N_2$ phase inside the composites remains unchanged. The results indicate that the oxidation of the $Y_{10}Si_6O_{24}N_2$ phase may occur through a diffusion reaction. After extended thermal exposure in air at 1400 °C, the $Y_{10}Si_6O_{24}N_2$ phase in the composite may decompose completely. From above results, it is obvious that composite containing the Si_2N_2O, $Y_2Si_2O_7$ or both Si_2N_2O and $Y_2Si_2O_7$ phases will exhibit better oxidation resistance, which is similar to those results reported by Lange *et al.* [21].

3.3. Mechanical properties

The room-temperature mechanical properties of the SiC_w/Si_3N_4 composites are summarized in Table VI. The flexural strength of the HP composites measured by three-point bending varied from 570–718 MPa. The fracture surfaces of the composite examined by SEM are shown in Fig. 11. Some whisker aggregation was observed on the fracture surface. Cracks initiated at the micro-pores around the whisker aggregation area led to the fracture of the composite. Furthermore, whisker pull-out was not observed on the fracture surface of the composites.

The fracture toughness values measured by both the chevron-notch beam technique and indentation test are also listed in Table VI. The fracture toughness measured using chevron-notch beam technique varied

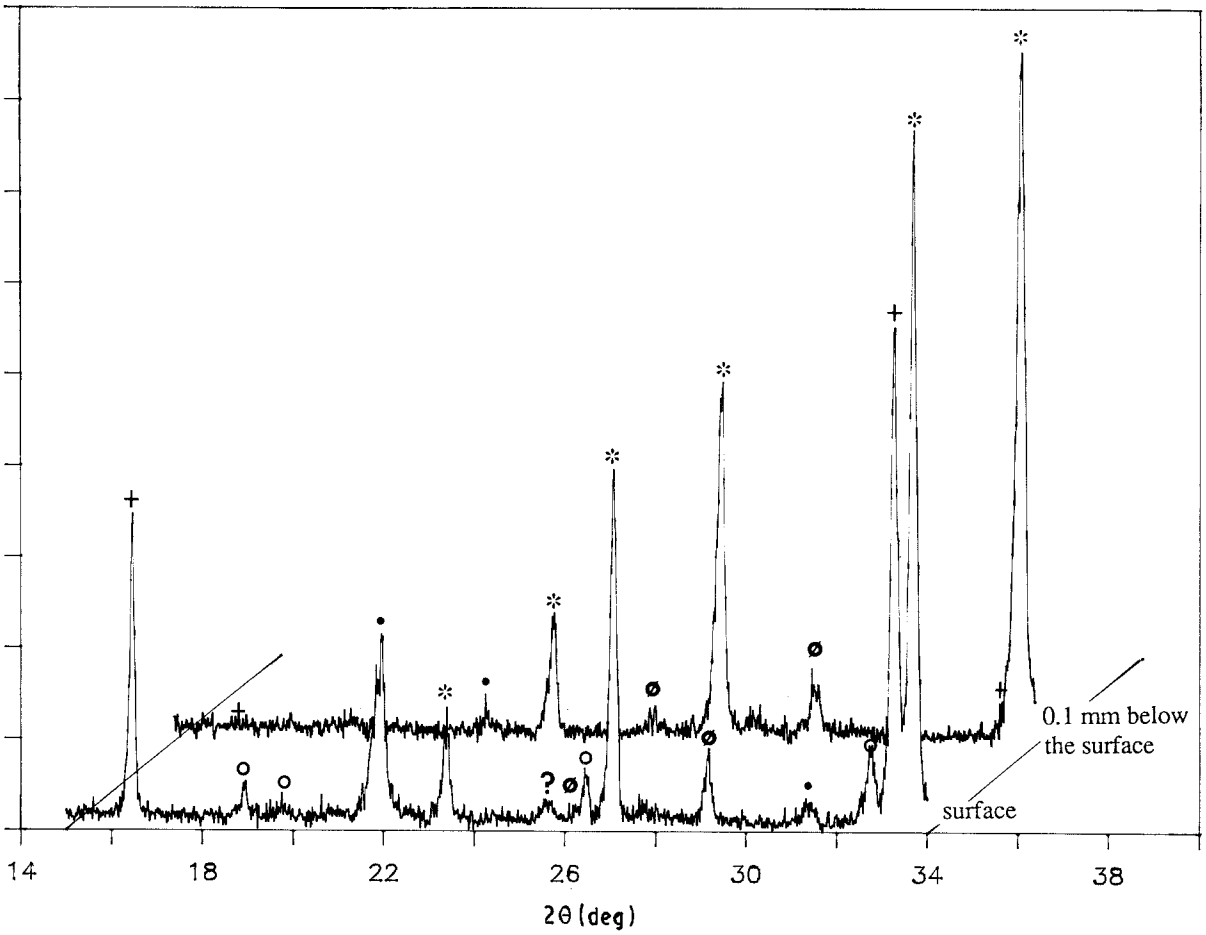

Figure 9 Typical XRD analysis of composite C after CTE testing (⁂) β-Si_3N_4, (○) Si_2N_2O, (+) β-$Y_2Si_2O_7$, (Ø) SiO_2 (coesite), (●) SiO_2 (cristobalite).

TABLE VI Mechanical properties of SiC_w/Si_3N_4 composites with different sintering additives

Composite grade	Flexural strength (MPa)	Weibull modulus	Fracture[a] toughness (MPa $m^{1/2}$)	
			(1)[a]	(2)[b]
A	617.6 (33.1)	14.50	6.85 (0.55)	6.81 (0.54)
B	633.8 (43.6)	11.54	7.21 (0.38)	7.34 (0.44)
C	570.4 (62.4)	7.65	6.87 (0.75)	–
D	718.5 (91.3)	5.92	6.64 (0.40)	7.07 (0.60)
E	665.2 (42.0)	12.23	7.83 (0.54)	–
F	675.9 (58.0)	8.75	7.60 (0.27)	7.22 (0.49)
G	611.1 (65.8)	7.18	7.57 (0.46)	–

[a] Three-point bending with chevron notch.
[b] Indentation method.

from 6.64–7.83 MPa $m^{1/2}$. The results of the indentation test are very similar to those obtained from the chevron-notch bending test. The micrographs of local indented areas examined by optical microscopy and SEM, are shown in Fig. 12a and b. Most of the cracks cut through the whisker near the sharp indented region because of the high stress concentration. However, the whiskers away from the sharp indented region remained intact. Whisker bridging, together with debonding at the matrix/whisker interface, appeared to be the major toughening mechanisms.

The results indicate that the amount of sintering additives does not significantly affect the mechanical properties of the composites at room temperature. However, it is well known that the amount and viscosity of the grain-boundary phases will significantly affect the mechanical behaviour of Si_3N_4 at elevated temperatures [22]. In addition, the residual stresses resulting from the thermal expansion mismatch between the Si_3N_4, SiC and grain-boundary phases may affect the crack propagation behaviour. Work is in progress to characterize further the effect of sintering additives on the mechanical behaviour of the composites at elevated temperatures.

4. Conclusions

1. A certain amount of SiC whiskers will degradate during the processing of the composite. The degree of whisker degradation is dependent upon the processing conditions and matrix composition (sintering additives).

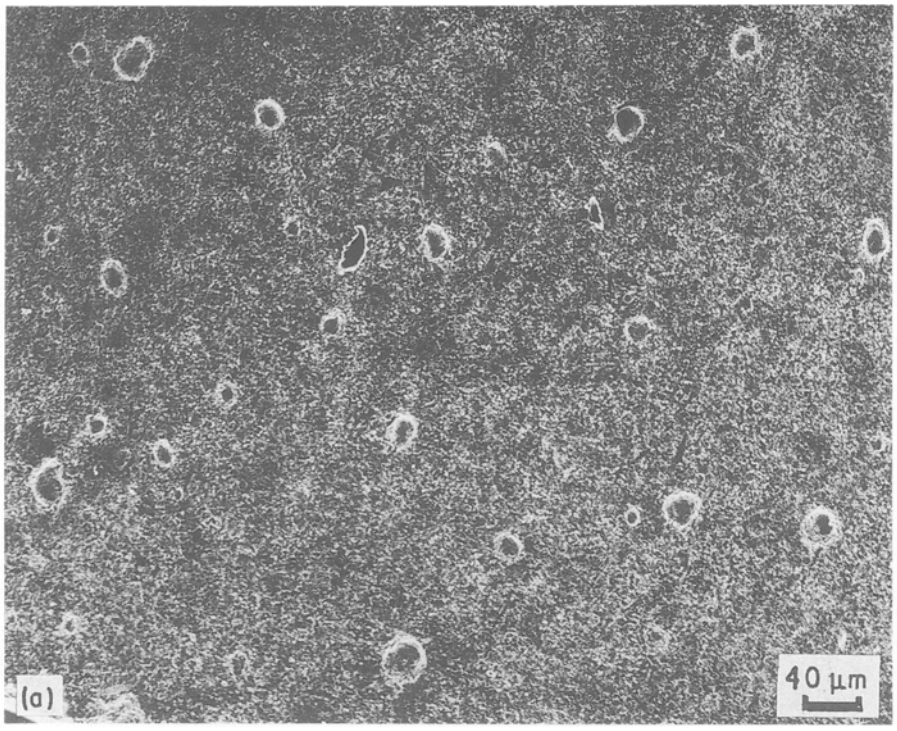

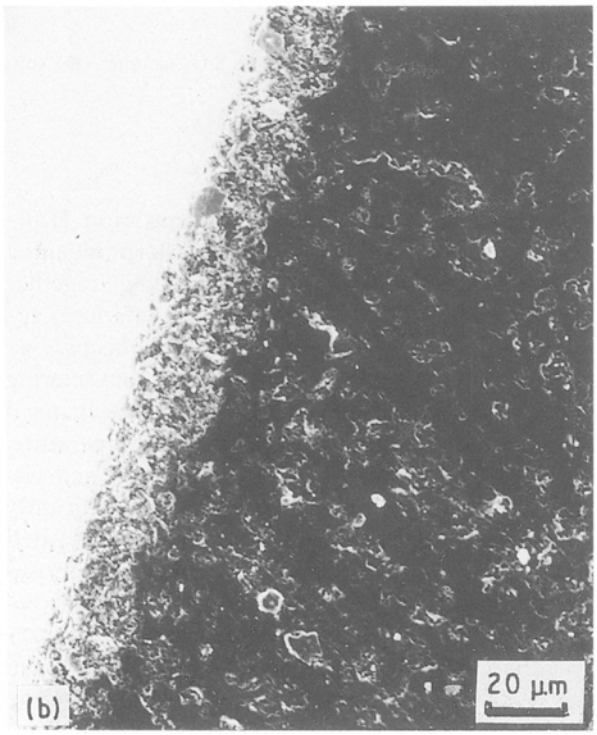

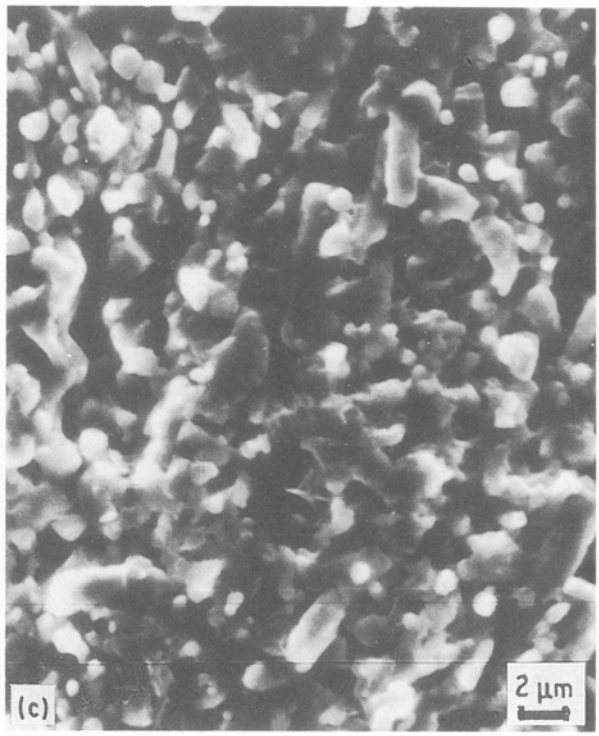

Figure 10 Scanning electron micrographs of composite L› after CTE testing: (a) porous structure of the oxide scale (top view); (b) cross-sectional view; (c) detail morphology of the oxide layer at the surface.

2. The sintering additives will affect the amounts and types of the crystallized grain-boundary phase in the matrix which, in turn, will affect the oxidation resistance of the composite. Composites containing the Si_2N_2O, $Y_2Si_2O_7$, or both Si_2N_2O and $Y_2Si_2O_7$ phases will exhibit better oxidation resistance while composites containing the $Y_{10}Si_6O_{24}N_2$ phase will be oxidized and form $Y_2Si_2O_7$ phase.

3. The amount of sintering additives does not significantly affect the mechanical properties of the composites at room-temperature. However, the sintering additives will affect the amount and viscosity of the

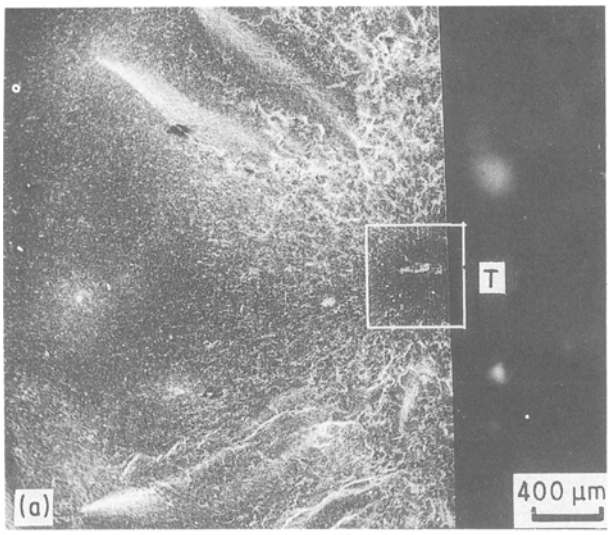

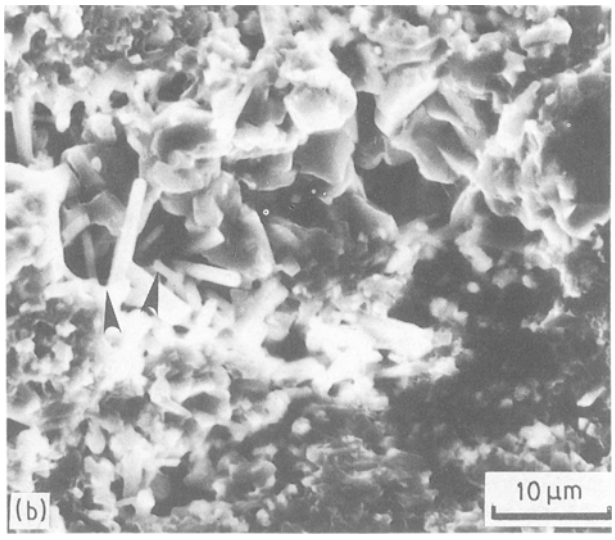

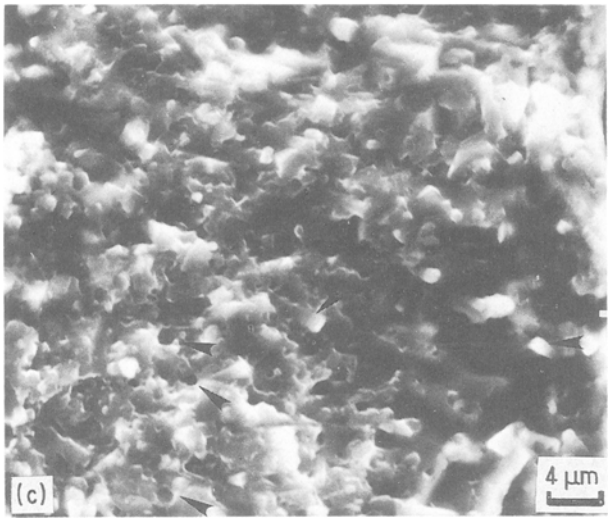

Figure 11 Fractography of SiC_w/Si_3N_4 composites: (a) fracture initiation; (b) whisker aggregation in the initiation area (white block in (a)); (c) whisker pull-out (arrows). T, tensile surface.

grain-boundary phases which, in turn, may affect the mechanical behaviour of the composites at elevated temperatures.

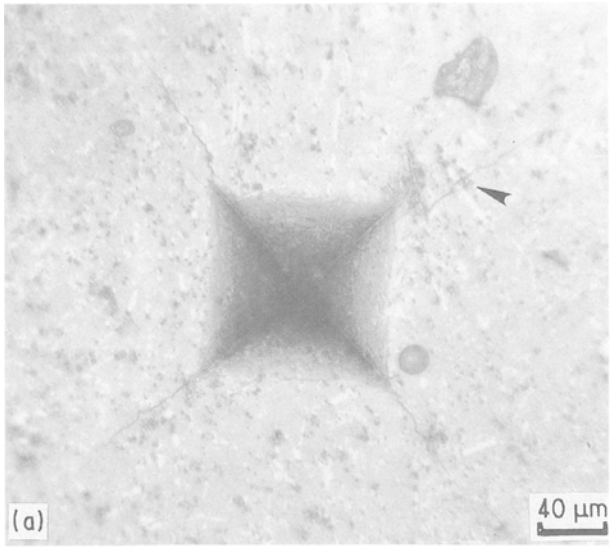

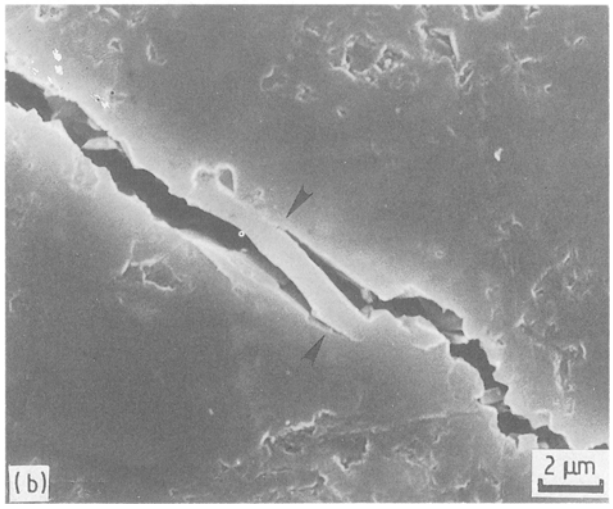

Figure 12 The crack propagation pattern: (a) near the indented area (arrow shows the crack through the whisker), (b) whisker-bridging along with debonding at the matrix/whisker interface (arrows) far away from the indented area.

Acknowledgement

This work was partially supported by the National Science Foundation (MSS-9057030).

References

1. P. F. BECHER and T. N. TIEGS, "Engineering Materials Handbook", Vol. 1, "Composites" (ASM International, Materials Park, OH, 1987) p. 941.
2. R. WARREN and V. K. SARIN, in "Applications of Fracture Mechanics to Composite Materials", edited by K. Friedrich (Elsevier Science, Amsterdam, 1989) p. 571.
3. S.-T. BULJAN, A. E. PASTO and H. J. KIM, *Amer. Ceram. Soc. Bull.* **68** (1989) 387.
4. R. HAYAMI, K. UENO, N. TAMARI and Y. TOIBANA, in "Tailoring Multiphase and Composite Ceramics", edited by R. Tressler and G. Messing (Plenum Press, New York, 1986) p. 663.
5. S. T. BULJAN and V. K. SARIN, in "Sintered Metal-Matrix Composite", edited by G. S. Upadhyaya (Elsevier Science, Amsterdam, 1984) p. 45.
6. P. F. BECHER, T. N. TIEGS, J. C. OGLE and W. H. WARWICK, in "Fracture Mechanics of Ceramics", Vol. 7, edited by R. C. Bradt, A. G. Evans, D. P. H. Hasselman and F. F. Lange (Plenum, New York, 1985) p. 61.

7. J. P. SINGH, K. C. GORETTA, D. S. KUPPERMAN, J. L. ROUTBORT and J. F. RHODES, *Adv. Ceram. Mater.* **3** (1988) 357.
8. H. M. JENNINGS, *J. Mater. Sci.* **18** (1983) 951.
9. C. J. SHIH, J. M. YANG and A. EZIS, *Ceram. Engng Sci. Proc.* **10** (1989) 1064.
10. C. P. GAZZARA and D. R. MESSIER, *Amer. Ceram. Soc. Bull.* **56** (1977) 777.
11. "1989 Annual Book of ASTM Standards", Vol. 03.01 (ASTM Easton, MD, 1989).
12. D. K. SHETTY, A. R. ROSENFIELD and W. H. DUCKWORTH, *J. Amer. Ceram. Soc.* **68** (1985) C-282.
13. M. K. CINBULK, G. THOMAS and S. M. JOHNSON, *J. Am. Ceram. Soc.* **73** (1990) 1606.
14. K. H. JACK, in "Nitrogen Ceramics", edited by F. L. Rieley (Noordhoff International, Reading, MA, 1977) p. 109.
15. S. A. BRADLEY, K. R. KARASEK, M. R. MARTIN, H. C. YEH and J. L. SCHIENLE, *J. Amer. Ceram. Soc.* **72** (1989) 628.
16. V. K. SARIN and M. RUHLE, *Composites* **18** (1987) 129.
17. M. E. WASHBURN, *Amer. Ceram. Soc. Bull.* **46** (1967) 667.
18. R. R. WILLS, S. HOLMQUIST, J. M. WIMMER and J. A. CUNNINGHAM, *J. Mater. Sci.* **11** (1976) 1305.
19. I. SEKERCIOGLU and R. R. WILLS, *J. Amer. Ceram. Soc.* **62** (1979) 590.
20. J. ITO and H. JOHNSON, *Amer. Mineral.* **53** (1968) 1940.
21. F. F. LANGE, S. C. SINGHAL and R. C. KUZNICKI, *J. Amer. Ceram. Soc.* **60** (1977) 249.
22. R. F. DAVIS and C. H. CARTER Jr, in "Advanced Ceramics", edited by S. Saito (Oxford University Press and Ohmsha Ltd, Oxford, 1988).

Received 21 March
and accepted 1 July 1991